Chemistry–A European Journal

Research Article
doi.org/10.1002/chem.202402793

**Chemistry
Europe**
European Chemical
Societies Publishing

www.chemeurj.org

Model Catalytic Studies on the Thermal Dehydrogenation of the Benzaldehyde/Cyclohexylmethanol LOHC System on Pt(111)

Valentin Schwaab,[a, b] Felix Hemauer,[a, b] Julien Steffen,[c, d] Natalie J. Waleska-Wellnhofer,[a] Eva Marie Freiberger,[a] Marius Steinmetz,[a] Andreas Görling,[c, d] Peter Wasserscheid,[e, f] Hans-Peter Steinrück,[a] and Christian Papp*[b]

We investigated the dehydrogenation reaction and the thermal robustness of the liquid organic hydrogen carrier (LOHC) couple benzaldehyde/cyclohexylmethanol on a Pt(111) model catalyst *in situ* in synchrotron radiation photoelectron spectroscopy- and complementary temperature-programmed desorption experiments. The system stores hydrogen in a cyclohexyl group and a primary alcohol functionality and achieves an attractive hydrogen storage capacity of 7.0 mass%. We observed a stepwise dehydrogenation mechanism, characterized by a low temperature dehydrogenation of the alcohol group at 235 K. However, stability limitations challenge the system's application as reversible hydrogen storage solution, as the resultant aldehyde was found to decompose during the dehydrogenation of its cyclohexyl group (between 250 and 350 K). A comparison of cyclohexylmethanol with the structurally related secondary alcohol (1-cyclohexylethanol; 6.3 mass% hydrogen) revealed a parallel stepwise dehydrogenation pattern for both compounds, but a technically relevant superior thermal robustness of the latter, demonstrating the influence of the alcohol-group's substitution degree on the dehydrogenation characteristics of alcohol-functionalized LOHCs. Density functional theory calculations are in agreement with the experimentally observed stability trend.

Introduction

Hydrogen is widely recognized as an extremely attractive energy vector for a future sustainable and renewable-based energy system.[1] With a gravimetric energy content nearly three times that of gasoline, elemental hydrogen can be readily produced by water electrolysis. This process enables the long-term storage of excess renewable energy on a large scale and thereby provides an effective means to mitigate natural power fluctuations, which are typically associated with renewable resources. On demand, the stored energy can be released again, for example through the cold combustion of hydrogen in a fuel cell, with water liberated as the only byproduct. However, elemental hydrogen is difficult to handle.[1d,2] The low density of the gas at ambient conditions (0.0898 $g\,L^{-1}$ at 0°C, 0.1 MPa) requires high levels of compression to achieve technologically relevant volumetric energy contents, and the established measures to realize this – i.e., storing H_2 under high pressures (35–70 MPa) or in the liquefied state at −253°C – involve significant energetic expenses and require a new and costly infrastructure.

Chemical storage methods aim to circumvent these challenges by binding hydrogen to a carrier compound. In the concept of liquid organic hydrogen carriers (LOHCs), H_2 is covalently bound to an organic liquid in an exothermic catalytic hydrogenation reaction.[3] The resulting hydrogen-rich liquids offer high volumetric energy contents under ambient conditions (~1.5–2 $kWh\,L^{-1}$, with hydrogen capacities of 5–7 mass%) and can be stored and transported in standard fuel tanks for crude oil derivatives (such as gasoline or diesel). After their endothermic catalytic dehydrogenation, the released H_2 is available for combustion or electrification, while the now hydrogen-lean compounds are recycled; in other words, the LOHC system functions as reusable liquid bottle for H_2. The complete storage cycle comprises two chemical species: the hydrogen-lean (H0-) and the hydrogen-rich (Hx-) form of the carrier.

[a] V. Schwaab, F. Hemauer, N. J. Waleska-Wellnhofer, E. Marie Freiberger, M. Steinmetz, H.-P. Steinrück
Lehrstuhl für Physikalische Chemie II, Friedrich-Alexander-Universität Erlangen-Nürnberg (FAU), Egerlandstr. 3, Erlangen 91058, Germany

[b] V. Schwaab, F. Hemauer, C. Papp
Angewandte Physikalische Chemie, Freie Universität Berlin (FU Berlin), Arnimallee 22, Berlin 14195, Germany
E-mail: christian.papp@fu-berlin.de

[c] J. Steffen, A. Görling
Lehrstuhl für Theoretische Chemie, Friedrich-Alexander-Universität Erlangen-Nürnberg (FAU), Egerlandstr. 3, Erlangen 91058, Germany

[d] J. Steffen, A. Görling
Erlangen National High Performance Computing Center (NHR@FAU), Martensstr. 1, Erlangen 91058, Germany

[e] P. Wasserscheid
Forschungszentrum Jülich GmbH, Helmholtz-Institute Erlangen-Nürnberg for Renewable Energy (IEK-11), Cauerstr. 1, Erlangen 91058, Germany

[f] P. Wasserscheid
Lehrstuhl für Chemische Reaktionstechnik, Friedrich-Alexander-Universität Erlangen-Nürnberg (FAU), Egerlandstr. 3, Erlangen 91058, Germany

⊡ Supporting information for this article is available on the WWW under https://doi.org/10.1002/chem.202402793

Chem. Eur. J. 2024, 30, e202402793 (1 of 10)

© 2024 The Author(s). Chemistry - A European Journal published by Wiley-VCH GmbH

Chemistry–A European Journal

Research Article
doi.org/10.1002/chem.202402793

Chemistry Europe
European Chemical
Societies Publishing

While the endothermic nature of the dehydrogenation reaction ensures a safe handling of the Hx-LOHC without significant energy losses even over extended periods of time, the typically high dehydrogenation enthalpies (such as $+65.4 \, kJ \, mol^{-1}$ H_2 for the prominent LOHC couple dibenzyltoluene/perhydrodibenzyltoluene)[4] are commonly cited as the main drawback of this technology.[2a] As a result, research has focused on tackling this problem, e.g., (1) by clever integration of waste heat from the H_2 fuel cell reaction to power the dehydrogenation of the Hx-LOHC in the dehydrogenation unit, thereby enhancing the overall efficiency of the energy storage cycle,[5] or (2) by chemical modification of the molecular framework of the carrier compounds to directly lower their dehydrogenation enthalpies (specifically, by the integration of heteroatoms into, traditionally, pure hydrocarbon-based structures).[6]

In the latter context, alcohol-functionalized LOHCs and their hydrogen-lean carbonyl derivatives have recently attracted particular attention.[7] This is because alcohols typically dehydrogenate at comparatively low temperatures but – other than the previously investigated N-heterocycles[6b,c,8] – are not foreign to the established infrastructure for crude oil derivatives (oxidation is a very common process in nature). Alcohol functionalization of pure hydrocarbon-based LOHCs is, in principle, easily accessible through oxidation of the H0-species and subsequent reduction of the resulting carbonyl.[9] Zakgeym et al. demonstrated that these oxo-functionalized systems show highly attractive properties for technical applications and may even outperform their pure hydrocarbon-based derivatives in various aspects, using the example of benzophenone/dicyclohexylmethanol,[9d] an oxidized version of the LOHC pair diphenylmethane/dicyclohexylmethane.[10] Moreover, alcohol-functionalized LOHCs can potentially be directly electrified through selective oxidation in organic fuel cells, which is currently being researched in a novel direct LOHC fuel cell concept.[7b,11]

A comprehensive understanding of the (de)hydrogenation mechanism and the thermal robustness of these compounds is essential for the development of technologically relevant hydrogen carrier systems and their applications. However, oxo-functionalized LOHCs are still relatively unexplored. The required fundamental mechanistic insights can be obtained through surface science studies.

We have recently investigated the thermal dehydrogenation mechanism of the oxo-functionalized LOHC pair of acetophenone and 1-cyclohexylethanol (a secondary alcohol) in a temperature-programmed surface science study on Pt(111).[12] In this publication, we shift our focus to the structurally related primary alcohol, cyclohexylmethanol (H8-BA), and its hydrogen-lean counterpart benzaldehyde (H0-BA) (Figure 1). One general aim of this work was to gain insight in how the substitution level of the alcohol group affects the dehydrogenation characteristics of alcohol-functionalized LOHCs. Another interesting aspect about the benzaldehyde/cyclohexylmethanol couple is the exceptionally high hydrogen storage capacity of 7.0 mass%, which exceeds that of the previously investigated acetophenone/1-cyclohexylethanol couple (6.3 mass%) by ~11%.

To elucidate the dehydrogenation mechanism of the H0-BA/H8-BA couple and establish the stability limits of the individual
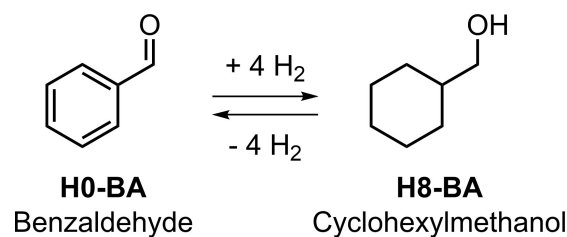
Figure 1. The benzaldehyde (H0-BA)/cyclohexylmethanol (H8-BA) LOHC system. Hydrogen is stored in two functionalities: a cyclohexyl group and a primary alcohol.
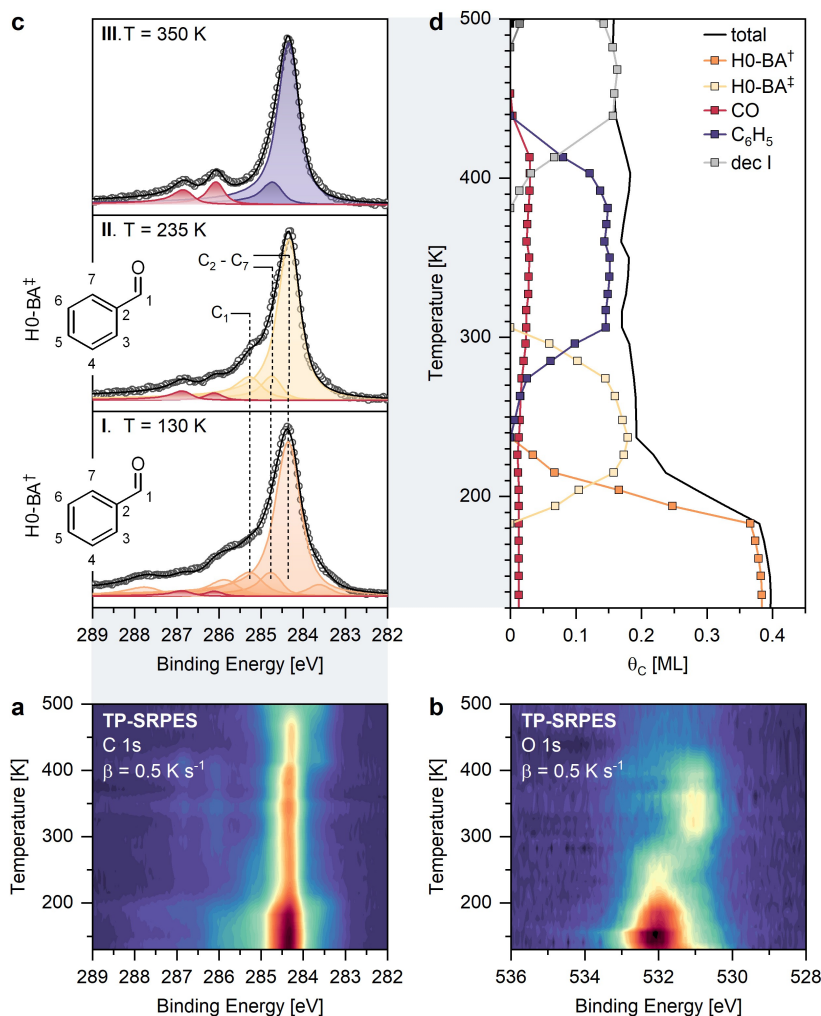
compounds under thermal dehydrogenation conditions, we conducted synchrotron radiation photoelectron spectroscopy (SRPES) and temperature-programmed desorption (TPD) experiments on a Pt(111) substrate. The substrate serves as well-defined model system for the more complex supported Pt catalysts that are commonly employed under practical dehydrogenation conditions.[13] A comparison of the results with those of our previous study on the acetophenone/1-cyclohexylethanol couple revealed a similar, stepwise dehydrogenation behavior for both primary and secondary alcohol, but crucial differences in the thermal robustness of both compounds, specifically with respect to their use as reversible hydrogen storage systems.

Results and Discussion

SRPES Results: Benzaldehyde (H0-BA) on Pt(111)

To determine the temperature boundaries for a reversible dehydrogenation of cyclohexylmethanol (H8-BA) on Pt(111), we first investigated the thermal robustness of the desired dehydrogenation product, benzaldehyde (H0-BA). Specifically, we monitored the thermal evolution of H0-BA on the model catalyst *in situ* in dedicated synchrotron radiation photoelectron spectroscopy (SRPES) experiments, both in the C 1s and the O 1s region. The spectra obtained during linear heating ($T_S = 130–550 \, K$, $\beta = 0.5 \, K \, s^{-1}$) are shown as color-coded density plots in Figure 2a (C 1s) and 2b (O 1s). For a detailed analysis of the different surface species, an appropriate fit model was introduced (Figure 2c and d); all peak parameters are listed in the SI (table S1).

The C 1s spectra obtained after adsorption of 0.39 C–ML of H0-BA at 130 K and subsequent annealing to 235 K are shown in Figure 2c (I and II, respectively). For reasons of simplicity, we start by addressing the latter: at 235 K, three peaks were introduced to fit the molecule-associated contributions, at 284.3, 284.7, and 285.2 eV [H0-BA‡] (Figure 2c, II). With an area ratio of 6:1, they are assigned to the phenyl carbon atoms (main peak at 284.3 eV and first vibrationally excited state at 284.7 eV) and the carbonyl carbon atom (285.2 eV) of the adsorbed compound.[10a,12] Further contributions at 286.1 and 286.8 eV are attributed to carbon monoxide impurities (CO_{bridge} and CO_{on-top}, respectively),[14] originating from the chamber background; at ~0.013 C–ML, they account for a negligible amount of ~3% of the total carbon coverage ($\theta_{C, total}$) at this point (Figure 2d).

Chemistry–A European Journal

Research Article
doi.org/10.1002/chem.202402793

Chemistry Europe
European Chemical
Societies Publishing

Figure 2. SRPES results for H0-BA on Pt(111). (**a** and **b**) Color-coded density plots of the C 1s (hν = 380 eV) and O 1s (hν = 650 eV) temperature-programmed XPS experiments (β = 0.5 K^{-1}); initial surface coverages after H0-BA adsorption at 130 K were ~0.39 and 0.38 C–ML, respectively. (**c**) Selected, individual XP spectra from the C 1s experiment with the applied fit model. (**d**) Corresponding quantitative analysis of the C 1s experiment, including the legend, which explains the color code of the fit model.

In order to achieve a satisfactory fit below 235 K, we had to introduce additional peaks at 283.6, 285.8, and 287.7 eV (Figure 2c, I). The broad line shape at this temperature (compared to the 235 K spectrum in Figure 2c, II) is attributed to the initial presence of multiple coexisting adsorption geometries (essentially different H0-BA species) on the surface. Coexisting binding motifs have already been reported for various adsorbates on low-index single crystal surfaces:[14,15] most relevant for the present study, for the closely related system of acetophenone on Pt(111), Attia and Schauermann observed the simultaneous presence of a flat-lying species and a weaker bound tilted species in IRAS experiments.[16] Typically, this phenomenon occurs after adsorption at low temperatures, where the mobility of the adsorbate and related surface processes, such as rearrangement or desorption, are thermally restricted. Consistent with this interpretation, we found that ~50% of the adsorbed H0-BA molecules (presumably weaker bound species) had desorbed at ~235 K (Figure 2d). In the fit model, we distinguished two "adsorption states": (i) multiple coexisting binding motifs below 235 K [H0-BA†] (Figure 2c, I), and (ii) the

most stable remaining binding motif above 235 K [H0-BA‡] (Figure 2c, II). Please note that the initial surface coverage of ≤ 0.39 C–ML strongly suggests that H0-BA† is a monolayer state. Further evidence for this assumption was obtained in a comparative analysis of the H0-BA† line shape with an additional high-exposure adsorption experiment, where we observed significant broadening and an overall shift to higher binding energies of the C 1s features, typical indicators for multilayer growth, only for coverages > 0.6 C–ML (SI, Figure S1). A precise assignment of the six H0-BA† peaks was still omitted, as we expect overlapping contributions of the different adsorption motifs. Moreover, it should be mentioned that the CO peaks (286.1 and 286.8 eV) were not resolved here due to their spectral overlap with the high binding energy features of H0-BA† (285.8 and 287.7 eV). Thus, below 235 K, CO$_{bridge}$ and CO$_{on-top}$ were fitted at a fixed intensity, determined from the spectrum in Figure 2c (II).

In the O 1s experiment, the adsorption of a comparable amount of H0-BA (0.38 C–ML) resulted in a broad line shape at 130 K, characterized by a dominant signal at 532.0 eV and a

Chemistry–A European Journal

Research Article
doi.org/10.1002/chem.202402793

**Chemistry
Europe**
European Chemical
Societies Publishing

shoulder at 530.6 eV (Figure 2b). Annealing to 235 K resulted in a narrowing of this line shape, as the shoulder at 530.6 eV diminished. We found that ~59% of the oxygen-containing species had desorbed at this point. As for the C 1s experiment, these changes are attributed to the desorption of weaker bound H0-BA species. Although desorbing water impurities might have contributed to some extent (see discussion of the O 1s experiment in the section "SRPES results: cyclohexylmethanol (H8-BA) on Pt(111)" and Figure S5 in the SI),[17] the matching relative intensity loss in both core levels (50% in the C 1s region versus 62% in the O 1s region, for a very similar initial carbon coverage) strongly indicates that the desorbing species was primarily H0-BA. The remaining signal above 235 K is attributed to the most stable remaining binding motif, H0-BA‡.

From Figure 2d, we deduce that H0-BA‡ was stable up to ~270 K. Heating above this temperature resulted in a rapid growth of the CO contributions in the C 1s region (286.1 and 286.8 eV) at the expense of the H0-BA‡ carbonyl peak (285.2 eV) (Figure 2a). Further confirmation of the decomposition of the molecule was obtained in the independent O 1s experiment, where we mainly observed the formation of CO_{bridge} with a contribution at 530.9 eV and, less pronounced, CO_{on-top} at 532.8 eV, at the expense of the H0-BA‡ carbonyl signal at 532.0 eV (Figure 2b).[18] Based on the C 1s line shape at 350 K, which differs from that of H0-BA‡ only in the absence of the carbonyl peak (285.2 eV) and the presence of two strong CO contributions (286.1 and 286.8 eV)[14] (Figure 2c, III), we reason that H0-BA‡ had decomposed into CO and a phenyl fragment $[C_6H_5]$ (fitted with a dominating peak at 284.3 eV and its vibrational satellite at 284.7 eV).[10a,19] Further changes at ~400 K (Figure 2a) are attributed to the decomposition of this C_6H_5 species into smaller, unspecified C–H fragments [dec I] (Figure 2d).[10a,12] CO was found to desorb until ~430 K,[20] as concluded from the absence of the corresponding contributions in both the C 1s and O 1s region above this temperature (Figure 2a and b).

From the falling edge of the H0-BA‡ curve in Figure 2d, we estimate a reaction temperature (at half maximum) of ~290 K for the decomposition of H0-BA‡. Assuming first order kinetics and a frequency factor of $\nu = 10^{13} s^{-1}$, this value can be translated to a reaction energy of ~0.82 eV, using the Redhead equation ($\beta = 0.5 \ K s^{-1}$).[21]

SRPES Results: Cyclohexylmethanol (H8-BA) on Pt(111)

Subsequently, we studied the thermal dehydrogenation of cyclohexylmethanol (H8-BA) on Pt(111) by SRPES. The results of the temperature-programmed experiments ($T_S = 130$–550 K, $\beta = 0.5 \ K s^{-1}$) are summarized in Figure 3. Additional spectra acquired during the initial adsorption process and the peak parameters of the employed fit model are again provided in the SI (Figure S2 and Table S2, respectively).
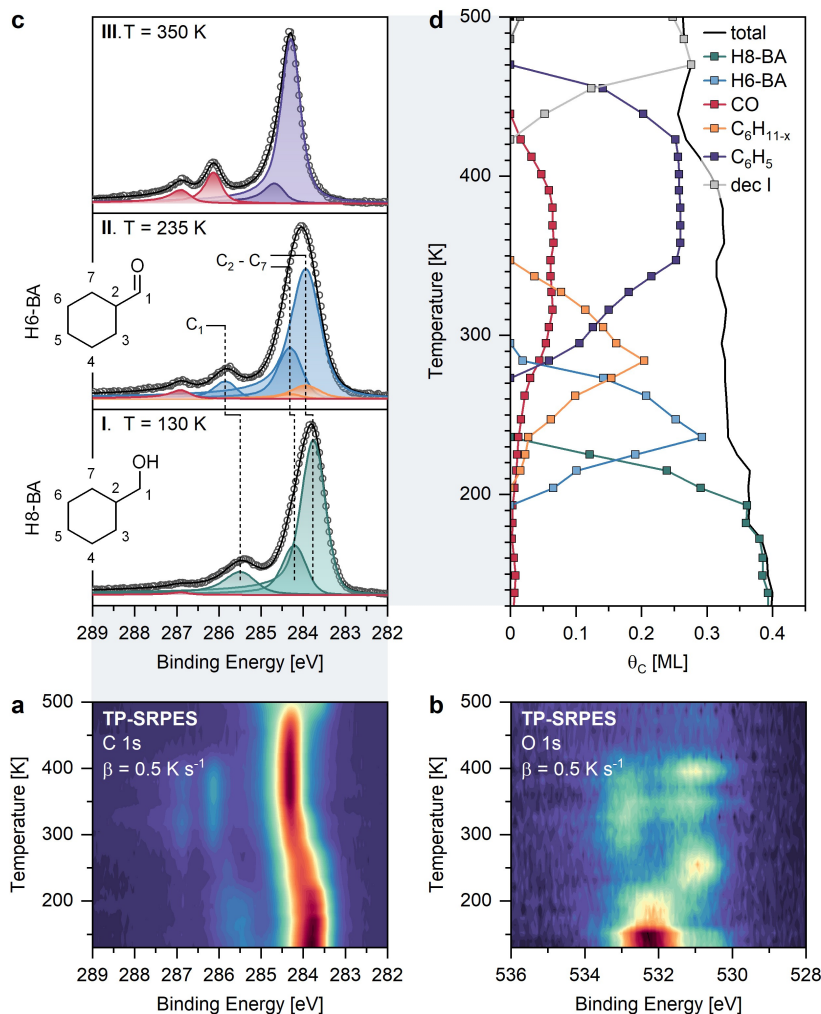
Figure 3c (I) shows the C 1s spectrum obtained after adsorption of 0.40 C–ML of H8-BA on Pt(111) at 130 K. The spectrum was fitted with three peaks, which were attributed to the cyclohexyl group (main peak at 283.7 eV and vibrational satellite at 284.2 eV) and the methanol subunit (285.4 eV) of H8-BA.[10a,12] The area ratio of the peaks was found to be 6:1 (283.7

and 284.2 eV combined, versus 285.4 eV), which is in perfect agreement with the stoichiometry of the molecule. The weak signal at 286.8 eV is again ascribed to contaminant carbon monoxide (CO_{on-top}),[14,18] which here accounts for <2% of the total carbon coverage (Figure 3d). Although it would not notably affect the fit model, it should be mentioned that a similar amount of CO_{bridge}, if it was present, would likely not be spectroscopically resolved at this point due to an overlap of the respective contribution (286.1 eV) with the methanol carbon signal of H8-BA (285.4 eV).

In the O 1s experiment, the adsorption of a comparable amount of H8-BA (0.38 C–ML) led to the evolution of a dominant signal at 532.2 eV with a shoulder at 530.6 eV (Figure 3b). Subsequent annealing to 160 K resulted in a narrowing of this line shape, as the main signal at 532.2 eV lost about ~48% of its intensity and the shoulder at 530.6 eV disappeared. We found that ~56% of the oxygen-containing species had desorbed at this point. Notably, this time, there were no signs of desorption in the C 1s experiment in this temperature range (Figure 3d). We thus attribute these findings to the desorption of co-adsorbed water, a common impurity in alcohols (likely originating from contact of the substance with air or the chamber background), with a contribution at 532.2 eV according to literature.[17] The shoulder at 530.6 eV could thereby be explained by a different chemical environment of H8-BA's oxygen atom (a second H8-BA species) due to an interaction with water molecules. Above 160 K, we observed only one oxygen signal at 532.1 eV, which is assigned to the methanol group of H8-BA.

First significant changes indicative of a surface reaction were found in both core levels at ~235 K. In the C 1s experiment, we observed a shift of all LOHC-related contributions to higher binding energies (Figure 3a). In the O 1s experiment, the signal at 532.1 eV diminished at the expense of a new dominant signal at 531.0 eV with a shoulder at 533.0 eV (Figure 3b). In light of our previous study on the acetophenone/1-cyclohexylethanol LOHC system, where we observed similar spectral changes upon the dehydrogenation of the alcohol moiety of 1-cyclohexylethanol on Pt(111) at ~210 K,[12] we analogously attribute the findings here – aside from the signal at 533.0 eV (discussed below) – to the dehydrogenation of the alcohol moiety of H8-BA. The proposed reaction product, cyclohexanecarboxaldehyde, was fitted with three new peaks at 283.9, 284.3, and 285.8 eV [H6-BA] (Figure 3c, II). These three peaks are attributed to the cyclohexyl group (283.9 and 284.3 eV)[10a] and the newly formed aldehyde group (285.8 eV) of the molecule, respectively.

The aforementioned shoulder at 533.0 eV (Figure 3b) is ascribed to CO_{on-top}.[14,18] Here, we propose the onset of a competing decomposition reaction, further indicated by an increasing CO coverage in the C 1s experiment in this temperature range. Notably, the inflection point of the CO coverage, θ_{CO}, in the quantitative analysis suggests that this fragmentation primarily occurred at a later stage of the heating experiment, around ~270 K (Figure 3d). This temperature range also aligns with the evolution of the CO_{on-top} signal in the O 1s region at 532.8 eV (Figure 3b). We highlight this observation, because it indicates that the fragmentation competes primarily with the further dehydro-

Chemistry–A European Journal

Research Article
doi.org/10.1002/chem.202402793

Chemistry Europe
European Chemical
Societies Publishing

Figure 3. SRPES results for H8-BA on Pt(111). (**a** and **b**) Color-coded density plots of the C 1s (hν = 380 eV) and O 1s (hν = 650 eV) temperature-programmed XPS experiments (β = 0.5 K⁻¹); initial surface coverages after H8-BA adsorption at 130 K were ~0.40 and 0.38 C–ML, respectively. (**c**) Selected, individual XP spectra from the C 1s experiment with the applied fit model. (**d**) Corresponding quantitative analysis of the C 1s experiment, including the legend, which explains the color code of the fit model.

genation of the intact LOHC, which we observed above ~250 K (discussed next).

Between ~250 and 350 K, we noted a gradual shift of the cyclohexyl contributions (283.9 and 284.3 eV) to higher binding energies (284.3 and 284.7 eV) (Figure 3a). Such behavior within this temperature range is typical for the Pt(111)-catalyzed dehydrogenation of cyclohexyl-based LOHCs to their respective phenyl species.[10a,12] We thus attribute this shift to the dehydrogenation of the cyclohexyl group of H6-BA. As previously indicated, the reaction appears to be accompanied by a fragmentation of the molecule, which manifests itself in an increasing CO coverage, particularly around 270 K (Figure 3d). Importantly, at 350 K, we again identified CO and C_6H_5 as the only remaining surface species, indicating that 100% of the molecules decomposed during their dehydrogenation. Decomposition of only partially dehydrogenated H6-BA (precisely, "H(6−x)-BA") would then result in CO and a partially dehydrogenated cyclohexyl species, C_6H_{11-x} (with $0 < x < 6$, depending on the progress of dehydrogenation). To distinguish this C_6H_{11-x} species quantita-

tively from H6-BA, we introduced an individual set of peaks in the fit model, starting at 283.9 and 284.3 eV [C_6H_{11-x}] (Figure 3c, II); for stoichiometric reasons, their area was correlated/restrained to the growth of the CO peaks, with a ratio of 6:1 (C_6H_{11-x} versus $CO_{on-top} + CO_{bridge}$). This model indicates the complete decomposition of H6-BA into CO and C_6H_{11-x}/C_6H_5 by ~300 K. The dehydrogenation of C_6H_{11-x} to C_6H_5 was found to occur until ~350 K. After that, we observed the same behavior as in the surface reaction of H0-BA, that is, further decomposition of C_6H_5 into unspecified C–H fragments [dec I],[10a,19] here around ~420 K (Figure 3d), and the complete desorption of CO from the catalyst's surface by ~430 K, as evident from the absence of the corresponding contributions in both binding energy regions (Figure 3a and 3b).

From Figure 2d, we estimate the following reaction temperatures: ~220 K for the dehydrogenation of H8-BA to H6-BA, ~275 K for the decomposition of H6-BA, and ~320 K for the complete dehydrogenation of C_6H_{11-x} to C_6H_5. Using the Redhead equation as in the previous section ($ν = 10^{13}$ s⁻¹, β =

Chem. Eur. J. **2024**, *30*, e202402793 (5 of 10)

© 2024 The Author(s). Chemistry - A European Journal published by Wiley-VCH GmbH

Chemistry–A European Journal

Research Article
doi.org/10.1002/chem.202402793

Chemistry
Europe
European Chemical
Societies Publishing

$0.5 \, K \, s^{-1}$),[21] these values can be translated to reaction energies of ~0.61, 0.77, and 0.90 eV, respectively.

TPD Results: Hydrogen Evolution from H0-BA and H8-BA on Pt(111)

We further analyzed the evolution of hydrogen (m/z = 2) from H0-BA and H8-BA on Pt(111) in complementary TPD measurements (Figure 4). (TPD curves for m/z = 28 confirming the evolution of CO are shown Figure S5 of the SI.)

For the hydrogen-lean molecule (orange), we observed two pronounced H_2 peaks with rate maxima at ~330 and 485 K, and a broad feature at ~530 K [H0-BA] (Figure 4). The first peak at ~330 K is assigned to the loss of a single hydrogen atom from the molecule's aldehyde moiety as it decomposes into CO and C_6H_5 (established in the section "SRPES results: benzaldehyde (H0-BA) on Pt(111)"). The difference in temperature compared to the decomposition maximum observed in SRPES (~290 K, estimated from the inflection point of the CO coverage; Figure 2d) is explained by the desorption temperature of hydrogen from Pt(111) (only above ~300 K, while the exact rate maximum is coverage dependent due to second order kinetics;[22] further discussed below), and the higher heating rate in TPD ($3 \, K \, s^{-1}$, compared to $0.5 \, K \, s^{-1}$ in the SRPES experiments). The second and third peak (at ~485 and 530 K) are attributed to the dehydrogenation of C–H fragments formed after further decomposition of C_6H_5 (around ~400 K). It should be noted that these smaller fragments were not distinguished in the fit model for the SRPES experiment due to their spectral overlap (Section A; Figure 2c and d). Therefore, this hydrogen release is not directly visible in the quantitative analysis in Figure 2d.

The H_2 TPD spectrum for H8-BA (green) differs from that for H0-BA only in the relative intensity and the rate maximum of the first desorption peak (H8-BA; Figure 4). With the SRPES results in mind, we conclude that this first signal, at ~305 K, corresponds to the loss of 9 out of the 14 hydrogen atoms from the adsorbed molecule; precisely, two hydrogen atoms due to the dehydrogenation of the alcohol moiety to an aldehyde group (at ~235 K), six hydrogen atoms due to the dehydrogenation of the cyclohexyl species to the respective phenyl (~250–

350 K), and one additional hydrogen atom due to the decomposition of the aldehyde species to CO and C_6H_5, respectively, C_6H_{11-x} (above ~260 K; established in the "SRPES results: cyclohexylmethanol (H8-BA) on Pt(111)" section). As hydrogen desorption occurs recombinatively, that is, following second order kinetics,[22] the rate maximum of this peak (at ~305 K) is shifted to lower temperatures relative to the first desorption peak in the H_2 spectrum for H0-BA (~330 K) due to the larger amount of hydrogen released in the H8-BA experiment. Above ~360 K, the H_2 TPD spectra for H0-BA and H8-BA are almost identical. This is in line with the SRPES results, where we found the same surface species, CO and C_6H_5, for both compounds above ~350 K (see Figure 2c, III and 3c, III).
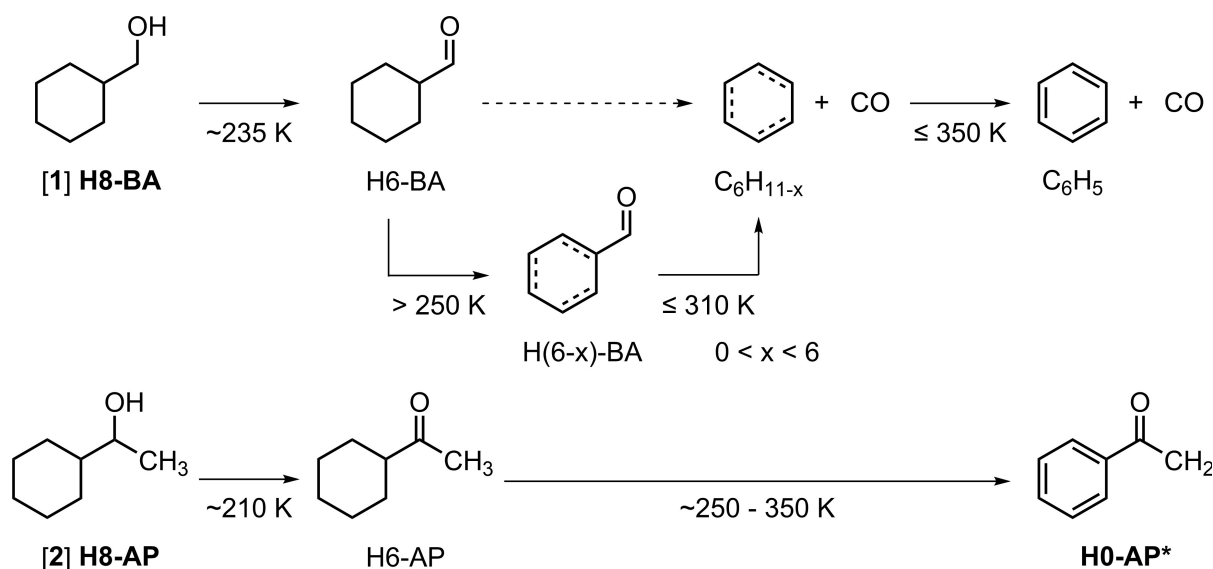
Primary- vs. Secondary Alcohol

In an attempt to establish how the degree of substitution of the alcohol group affects the dehydrogenation characteristics of alcohol-functionalized LOHCs, we compared the results for cyclohexylmethanol [1] (a primary alcohol) with those of our previous study on the structurally related secondary alcohol 1-cyclohexylethanol[12] [2]. Both compounds were studied in comparable temperature-programmed SRPES experiments on Pt(111) and differ only in one substituent of their alcohol group (1: –H versus 2: –CH_3).

We found a parallel stepwise dehydrogenation pattern for 1 and 2 (Figure 5). Both compounds dehydrogenated first at their alcohol group to the respective H6-carbonyl, at ~235 (1) and 210 K (2). The subsequent dehydrogenation of the cyclohexyl group was also observed within the same temperature window for both H6-BA and H6-AP, between ~250 and 350 K. However, while our previous study demonstrated that a complete dehydrogenation of 2 to the desired hydrogen-lean acetophenone (precisely, an acetophenone-like H0-AP* species, with a terminal CH_2 group) can be achieved without major decomposition of the carrier's carbon framework (under the applied model catalytic conditions), in our current study we found no H0-BA in the surface reaction of 1. Instead, we observed an early decomposition into CO and a (partially dehydrogenated) C_6H_{11-x} fragment competing with the desired dehydrogenation of intact H6-BA. Notably, this decomposition reaction was already completed (100% conversion of adsorbed LOHC into CO and C_6H_{11-x}/C_6H_5) at ~310 K, that is, before the complete dehydrogenation of the cyclohexyl group of H6-BA (expected to occur until ~350 K, based on the reaction path for 2 and the for 1 instead observed dehydrogenation of C_6H_{11-x}), so that no H0-BA was formed. In other words, our results suggest that a reversible dehydrogenation to the desired H0-LOHC is only possible for the secondary alcohol-functionalized compound (2) but not for the primary alcohol-functionalized one (1) due to an inferior thermal stability of the aldehyde intermediate (H6-BA) compared to the ketone (H6-AP) formed in the dehydrogenation sequence of 2.

To test this hypothesis, we performed DFT simulations to evaluate the thermodynamics of the dissociation of the aldehyde/ketone moiety from the cyclohexyl group of H6-BA
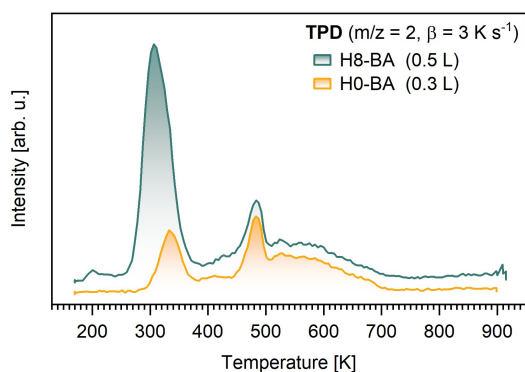
Figure 4. H_2 TPD curves for benzaldehyde (H0-BA) and cyclohexylmethanol (H8-BA) on Pt(111) after adsorption at 170 K; m/z = 2, $\beta = 3 \, K \, s^{-1}$.

Chemistry–A European Journal

Research Article
doi.org/10.1002/chem.202402793

Chemistry
Europe
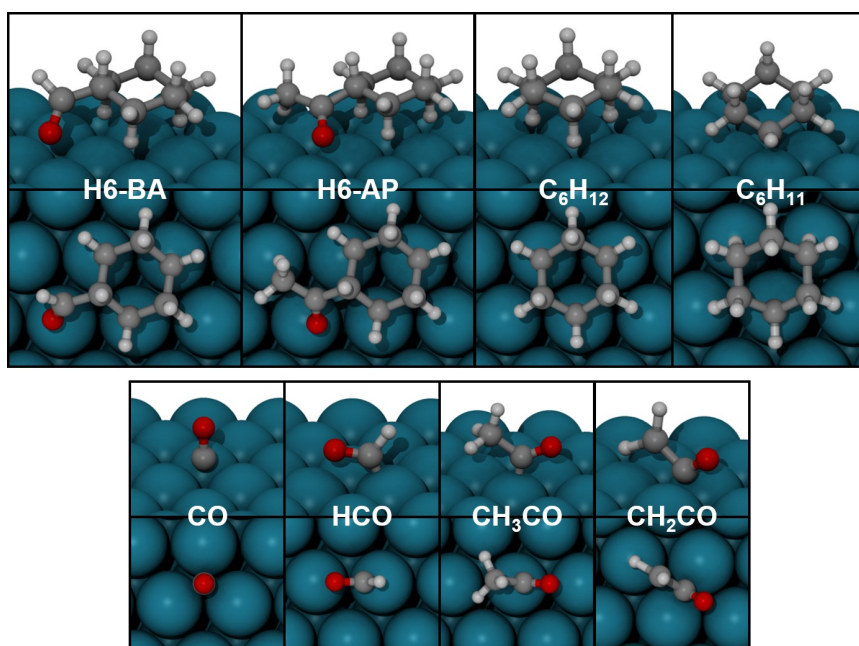European Chemical
Societies Publishing

Figure 5. Proposed reaction sequences for the thermal dehydrogenation of cyclohexylmethanol (H8-BA) [1] and 1-cyclohexylethanol [2] on Pt(111). The scheme was created on the basis of the experimental results presented in this work (**1**) and in our previous publication (**2**).[12]

and H6-AP in the gas phase and on the Pt surface. First gas phase simulations (optimized nudged elastic band reaction paths) confirmed that the decomposition of H6-BA is thermodynamically favored over that of H6-AP, provided that hydrogen atoms in the fragments can rearrange in such a way that the resulting products are C_6H_{12} and CO for H6-BA ($+0.36$ eV) and C_6H_{12} and CH_2CO for H6-AP ($+1.22$ eV) (see Table 1 and, in the SI, Figures S6 and S7). Further calculations were performed including the Pt(111) surface. For this extended system, calculations of the NEB reaction pathways were not done as they are computationally much more demanding than in the gas phase and likely include Pt atoms, leading to a larger space of possible reaction paths. Instead, the energies of all reactants and suggested products on the surface were calculated. Continuing the argument from our gas phase simulations, this allowed for a thermodynamic comparison of the addressed decomposition reactions. The optimized geometries and total energies of H6-BA, H6-AP, and of the possible decomposition products are shown in Figure 6 and Table 1. The main difference to the gas phase is that radicals are quenched and

stabilized at the surface. All calculations were done with consideration of spin-polarization, the resulting magnetic moments in all cells, however, were zero. The unpaired spins of the radical species were thus effectively quenched by the Pt(111) surface, leading to chemisorbed radical species. Closed-shell molecules (H6-BA, H6-AP, and C_6H_{12}) were only physisorbed, with the exception of CO chemisorbed in hollow position. In contrast to results obtained for the gas phase, the possible decomposition pathways were now all exothermic. The H6-BA decompositions, especially those to C_6H_{12} and CO, as well as to C_6H_{11}, H and CO, however, were still more favorable than the H6-AP decompositions, which is again in agreement with the experimental results. In both cases, the decompositions leading to C_6H_{11}, H, and CO/CH_2CO are slightly more favorable than those resulting in C_6H_{12}, probably due to chemisorption of the radical species on the Pt(111) surface, indicated by the high adsorption energies of them shown in Table S4. The differences in reaction energies, however, are small (0.1–0.2 eV), such that, in principle, both processes are expected to occur under experimental conditions. In fact, our experiment does not allow us to confirm or exclude either pathway ($C_6H_{11}+H$ or C_6H_{12}, respectively, C_6H_5+H or C_6H_6). It is also important to note that particularly in the gas phase, but also on the surface (due to weak interactions of the molecules with it), the reactions are still expected to be kinetically hindered. Nevertheless, thermodynamically, the results confirm that H6-BA is the less stable compound and prone to lose a CO molecule. Finally, it should be considered that the adsorption of CO on different metal surfaces is a known error source of many prominent DFT functionals.[23] In reality, CO prefers to adsorb on the top position on Pt(111), in contrast to the hollow position obtained in the calculations. Further, the overall binding energy is approximately 0.3–0.4 eV too high in comparison to the experiment. This leads to a slight overestimation of the favorability of the decomposition/rearrangement processes of H6-BA resulting

Table 1. Energy differences (products – reactants) of the proposed decomposition pathways, calculated in the gas phase (SI Figure S5) and for the reactants and products adsorbed on a Pt(111) surface (Figure 6, Table S2). Decomposition pathways resulting in three products were only calculated for the Pt(111) surface. In the gas phase calculation, C_6H_{11} and H would immediately recombine.

Reaction	ΔE_{vacuum} (eV)	$\Delta E_{Pt(111)}$ (eV)
H6-BA → C_6H_{11} + HCO	5.547	−0.739
H6-BA → C_6H_{11} + H + CO	-	−1.718
H6-BA → C_6H_{12} + CO	0.359	−1.513
H6-AP → C_6H_{11} + CH_3CO	5.453	−0.614
H6-AP → C_6H_{11} + H + CH_2CO	-	−0.703
H6-AP → C_6H_{12} + CH_2CO	1.216	−0.498

Chemistry–A European Journal

Research Article
doi.org/10.1002/chem.202402793

Chemistry Europe
European Chemical
Societies Publishing

Figure 6. Optimized adsorption geometries on Pt(111) of H6-BA, H6-AP, and of the different possible decomposition products occurring along the proposed decomposition pathways. The individual corresponding total energies are listed in the SI (Table S2).

in CO. Since the energetic advantage of these processes in comparison to a simple decomposition leading to HCO, however, is much larger than 0.3–0.4 eV (>0.8 eV in total), it is expected that the qualitative ordering of the reactions in the DFT calculations is not affected by it.

Conclusions

We studied the dehydrogenation reaction and thermal robustness of the LOHC couple H0-BA/H8-BA on a Pt(111) model catalyst surface *in situ* by SRPES and complementary TPD experiments. Our main conclusions are:

1. Hydrogen release from H8-BA proceeds in a stepwise manner, with the alcohol group dehydrogenating first at a very favorable temperature of 235 K. Further dehydrogenation at the cyclohexyl group of the resultant aldehyde (H6-BA) occurred gradually between 250 and 350 K.
2. Stability limitations challenge the reversibility of the hydrogen storage cycle. H6-BA was found to decompose during the dehydrogenation of its cyclohexyl group, resulting in CO and C_6H_{11-x}/C_6H_5 as the only remaining surface species at 300 K. Conversion to the desired product (H0-BA) was not observed.
3. A comparison of the results with the structurally related LOHC pair of acetophenone (H0-AP) and 1-cyclohexylethanol (H8-AP) revealed a parallel stepwise dehydrogenation pattern for both primary and secondary alcohol, but crucial differences in the thermal robustness of both compounds. Our previous study[12] demonstrated that a Pt(111)-catalyzed dehydrogenation to an acetophenone-like (H0-AP*) species can be achieved without significant decomposition of the

carrier's carbon framework, which contrasts the current results on the primary alcohol (H8-BA). DFT calculations are in agreement with the experimentally observed stability trends.

Our study contributes to a better understanding of the dehydrogenation behavior and thermal stability limits of alcohol-functionalized alicyclic LOHCs and their hydrogen-lean carbonyl derivatives on Pt-based dehydrogenation catalysts.

Experimental Section

Synchrotron Radiation Photoelectron Spectroscopy (SRPES)

All synchrotron radiation-based X-ray photoelectron spectroscopy experiments were conducted at the open-port beamline U49-2 PGM-1 of BESSY II (Helmholtz-Zentrum Berlin).[24] Our transportable UHV-apparatus is a two-chamber setup specifically designed for monitoring surface processes of adsorbates *in situ*; briefly, it features a hemispherical electron energy analyzer (Omicron EA125 U7 HR), an evaporator for organic compounds, a three-stage supersonic molecular beam, a sputter gun, and LEED optics. Further details on the apparatus are given elsewhere.[25]

A Pt(111) crystal served as model catalyst in all experiments (MaTecK, 99.999%, depth of roughness <0.01 μm, accuracy of orientation $<0.1°$). Prior to dosing a compound, the cleanness of the crystal was confirmed by XPS. Carbon residues from previous experiments were removed by oxidation at 850 K (O_2, 10 sccm direct exposure using the molecular beam) and subsequent annealing to 1050 K. Other contaminants were removed by sputtering (Ar^+, $E=1.0$ keV, I_S ~8 μA, 20 min) and subsequent annealing to 1200 K. Benzaldehyde (H0-BA, $\geq99\%$, Sigma-Aldrich, B1334) or cyclohexylmethanol (H8-BA, $\geq99\%$, Sigma-Aldrich, C105805), were then dosed onto the clean substrate at 130 K, using the organic evaporator, which utilizes the vapor pressures of the

Chemistry–A European Journal

Research Article
doi.org/10.1002/chem.202402793

Chemistry Europe
European Chemical
Societies Publishing

compounds. During this procedure, the adsorption process of the respective compound was monitored *in situ* by continuous XPS measurements, either in the C 1s or the O 1s region. Subsequently, the sample was heated with a linear heating ramp of 0.5 K s^{-1}, using a bifilar coil filament located at the back of the crystal. Throughout this heating process, the thermal evolution of the compound was again monitored *in situ* in the respective binding energy region by continuous XPS measurements at intervals of ≤ 15 K.[26]

For both compounds, dedicated experiments in the C 1s and the O 1s regions were carried out, with resolutions of ~160 and 250 meV, using excitation energies of 380 and 650 eV, respectively. The spectra were recorded at normal emission (0°), with a light-incident angle of 50°. To minimize beam damage, the position of the X-ray spot on the sample was shifted after each sweep by readjusting the crystal position in the x- or y- direction. The data was processed by referencing each spectrum to the Fermi level and subtracting a linear background. The spectra were then fitted with an appropriate set of peaks; the line shape was a convolution of Doniach-Šunjić[27] and Gaussian functions. For quantification, the C 1s peak intensities were referenced to that of a *c* (4×2)-CO superstructure on Pt(111),[14,28] which equals a carbon coverage of $\theta_C = 0.5$ C–ML (i.e., one carbon atom per two Pt-surface atoms).

Temperature-Programmed Desorption (TPD)

Temperature-programmed desorption experiments were performed in a stationary two-chamber UHV-setup in the lab in Erlangen. The apparatus is equipped with a laboratory X-ray source (SPECS XR50), a hemispherical electron analyzer (Omicron PN04635 Argus Spectrometer), a quadrupole mass spectrometer (Pfeiffer Vacuum QMS 200), a "Feulner cup",[29] an evaporation system for organic substances, a sputter gun, and LEED optics. A Pt(111) crystal was again used as model catalyst. Prior to each experiment, carbon residues were removed by oxidation at 900 K (O$_2$, indirect) and subsequent annealing to 1050 K. Other contaminants were removed by sputtering (Ar$^+$, E = 1.0 keV, I$_S$ ~2 μA, 80 min) and subsequent annealing to 1200 K. H0-BA or H8-BA were then dosed onto the substrate at 170 K. Subsequently, the substrate was heated linearly with a heating rate of 3 K s^{-1} and the desorbing species (for example, H$_2$ at m/z = 2) were monitored using the QMS.

Density Functional Theory (DFT)

Nonperiodic DFT calculations were done with the Orca 5.1 program.[30] The PBE functional[31] and a def2-TZVPP basis set were used. Dispersion effects were included with the DFT D4 correction scheme.[32] The bond dissociation scans were performed with 50 steps in total, varying the bond length between 1.35 and 6.0 Angstroms (Å). For the nudged elastic band (NEB) calculations of the rearrangement processes, the geometries of the reactants and the decomposed products were optimized first and then used as initial and final states of the NEB calculations. 30 NEB images were used for each calculation. The transition states of both rearrangements were optimized on the fly with the climbing image algorithm implemented into Orca. Periodic DFT modeling of the adsorbate systems was conducted with the VASP code, which employs a plane wave basis set for the description of the valence electrons in combination with the projector augmented wave (PAW) method for the representation of the atomic cores.[33] The kinetic energy cutoff was chosen to be 600 eV for geometry optimizations, and exchange correlation effects were treated with the PBE functional.[31] The DFT D3 correction with Becke-Johnson damping was used for better description of dispersion interactions.[34] Brillouin zone sampling was done with a Γ-containing 2×2×1 k-point mesh. A first order Methfessel-Paxton scheme[35] with a

broadening of 0.15 eV was applied to smear the electronic states for the geometry optimization, the tetrahedron smearing with Blöchl corrections[36] was applied for the calculation of energies for the optimized structures. A Pt(111) surface was built by first relaxing a bulk fcc Pt cell, resulting in a Pt—Pt distance of 2.804 Å. Pt(111) surface slabs were built with the optimized Pt—Pt distance, with the slabs comprising five layers in depth, of which the lowest two layers were frozen. In the z-direction, a vacuum of 21 Å length was introduced in order to avoid periodic interactions between slabs with adsorbates. The surface slab unit cell had a size of 6×6 Pt atoms per layer. The different initial adsorption geometries were built with the build adsorbates.py script from the VASP4CLINT GitHub repository [https://github.com/Trebonius91/VASP4CLINT]. Their geometries were optimized until all gradient components were below 0.02 eV Å^{-1}.

Conflict of Interests

The authors declare no conflict of interest.

Data Availability Statement

The data that support the findings of this study are openly available in Zenodo at https://doi.org/10.5281/zenodo.12801557, reference number 12801557.

[1] a) Bundesministerium für Wirtschaft und Klimaschutz (BMWK), "Die Nationale Wasserstoffstrategie", can be found under https://www.bmwk.de/Redaktion/DE/Publikationen/Energie/die-nationale-wasser-stoffstrategie.html, 2020 (accessed 1 October 2024); b) European Commission, "Hydrogen", can be found under https://energy.ec.europa.eu/topics/energy-systems-integration/hydrogen en, 2023 (accessed 1 October 2024); c) M. Hirscher, V. A. Yartys, M. Baricco, J. Bellosta von Colbe, D. Blanchard, R. C. Bowman, D. P. Broom, C. E. Buckley, F. Chang, P. Chen, Y. W. Cho, J.-C. Crivello, F. Cuevas, W. I. F. David, P. E. de Jongh, R. V. Denys, M. Dornheim, M. Felderhoff, Y. Filinchuk, G. E.

Froudakis, D. M. Grant, E. M. Gray, B. C. Hauback, T. He, T. D. Humphries, T. R. Jensen, S. Kim, Y. Kojima, M. Latroche, H.-W. Li, M. V. Lototskyy, J. W. Makepeace, K. T. Møller, L. Naheed, P. Ngene, D. Noréus, M. M. Nygård, S.-i. Orimo, M. Paskevicius, L. Pasquini, D. B. Ravnsbæk, M. Veronica Sofianos, T. J. Udovic, T. Vegge, G. S. Walker, C. J. Webb, C. Weidenthaler, C. Zlotea, *J. Alloys Compd.* **2020**, *827*, 153548; d) P. Preuster, A. Alekseev, P. Wasserscheid, *Annu. Rev. Chem. Biomol. Eng.* **2017**, *8*, 445–471.

[2] a) U. Eberle, M. Felderhoff, F. Schuth, *Angew. Chem. Int. Ed.* **2009**, *48*, 6608–6630; b) K. Müller, *ChemBioEng Rev.* **2019**, *6*, 72–80.

[3] a) P. Preuster, C. Papp, P. Wasserscheid, *Acc. Chem. Res.* **2017**, *50*, 74–85; b) D. Teichmann, W. Arlt, P. Wasserscheid, R. Freymann, *Energy Environ. Sci.* **2011**, *4*, 2767–2772; c) D. Teichmann, W. Arlt, P. Wasserscheid, *Int. J. Hydrog. Energy* **2012**, *37*, 18118–18132; d) P. M. Modisha, C. N. M. Ouma, R. Garidzirai, P. Wasserscheid, D. Bessarabov, *Energy Fuels* **2019**, *33*, 2778–2796; e) P. Rao, M. Yoon, *Energies* **2020**, *13*, 6040.

[4] K. Müller, K. Stark, V. N. Emel'yanenko, M. A. Varfolomeev, D. H. Zaitsau, E. Shoifet, C. Schick, S. P. Verevkin, W. Arlt, *Ind. Eng. Chem. Res.* **2015**, *54*, 7967–7976.

[5] a) P. Preuster, Q. Fang, R. Peters, R. Deja, V. N. Nguyen, L. Blum, D. Stolten, P. Wasserscheid, *Int. J. Hydrog. Energy* **2018**, *43*, 1758–1768; b) K. Müller, S. Thiele, P. Wasserscheid, *Energy Fuels* **2019**, *33*, 10324–10330.

[6] a) K. Müller, J. Völkl, W. Arlt, *Energy Technol.* **2013**, *1*, 20–24; b) E. Clot, O. Eisenstein, R. H. Crabtree, *Chem. Commun.* **2007**, *22*, 2231–2233; c) R. H. Crabtree, *Energy Environ. Sci.* **2008**, *1*, 134–138.

[7] a) A. Suárez, *Phys. Sci. Rev.* **2018**, *3*, 20170028; b) G. Sievi, D. Geburtig, T. Skeledzic, A. Bösmann, P. Preuster, O. Brummel, F. Waidhas, M. A. Montero, P. Khanipour, I. Katsounaros, J. Libuda, K. J. J. Mayrhofer, P. Wasserscheid, *Energy Environ. Sci.* **2019**, *12*, 2305–2314; c) V. Yadav, G. Sivakumar, V. Gupta, E. Balaraman, *ACS Catal.* **2021**, *11*, 14712–14726; d) Y. Q. Zou, N. von Wolff, A. Anaby, Y. Xie, D. Milstein, *Nat. Catal.* **2019**, *2*, 415–422; e) S. Schauermann, *ACS Catal.* **2023**, *13*, 13423–13433.

[8] a) C. Papp, P. Wasserscheid, J. Libuda, H. P. Steinrück, *Chem. Rec.* **2014**, *14*, 879–896; b) M. Schwarz, P. Bachmann, T. N. Silva, S. Mohr, M. Scheuermeyer, F. Späth, U. Bauer, F. Düll, J. Steinhauer, C. Hohner, T. Dopper, H. Noei, A. Stierle, C. Papp, H. P. Steinrück, P. Wasserscheid, A. Gorling, J. Libuda, *Chem. Eur. J.* **2017**, *23*, 14806–14818; c) P. Bachmann, M. Schwarz, J. Steinhauer, F. Späth, F. Düll, U. Bauer, T. Nascimento Silva, S. Mohr, C. Hohner, M. Scheuermeyer, P. Wasserscheid, J. Libuda, H. P. Steinrück, C. Papp, *J. Phys. Chem. C* **2018**, *122*, 4470–4479; d) J. Steinhauer, P. Bachmann, E. M. Freiberger, U. Bauer, H. P. Steinrück, C. Papp, *J. Phys. Chem. C* **2020**, *124*, 22559–22567; e) P. Bachmann, J. Steinhauer, F. Späth, F. Düll, U. Bauer, R. Eschenbacher, F. Hemauer, M. Scheuermeyer, A. Bösmann, M. Büttner, C. Neiss, A. Gorling, P. Wasserscheid, H. P. Steinrück, C. Papp, *J. Chem. Phys.* **2019**, *151*, 144711.

[9] a) M. Kerscher, J. H. Jander, J. Cui, M. M. Martin, M. Wolf, P. Preuster, M. H. Rausch, P. Wasserscheid, T. M. Koller, A. P. Fröba, *Int. J. Hydrog. Energy* **2022**, *47*, 15789–15806; b) D. Santhanaraj, C. Suresh, M. Guru-lakshmi, N. R. Sasirekha, K. Shanthi, *React. Kinet. Mech. Cat.* **2011**, *104*, 399–415; c) S. Devika, M. Palanichamy, V. Murugesan, *Chinese J. Catal.* **2012**, *33*, 1086–1094; d) D. Zakgeym, J. D. Hofmann, L. A. Maurer, F. Auer, K. Müller, M. Wolf, P. Wasserscheid, *Sustain. Energy Fuels* **2023**, *7*, 1213–1222.

[10] a) C. Gleichweit, M. Amende, O. Höfert, T. Xu, F. Späth, N. Brückner, P. Wasserscheid, J. Libuda, H.-P. Steinrück, C. Papp, *J. Phys. Chem. C* **2015**, *119*, 20299–20311; b) M. Amende, C. Gleichweit, T. Xu, O. Höfert, M. Koch, P. Wasserscheid, H. P. Steinrück, C. Papp, J. Libuda, *Catal. Lett.* **2016**, *146*, 851–860.

[11] a) M. Brodt, K. Müller, J. Kerres, I. Katsounaros, K. Mayrhofer, P. Preuster, P. Wasserscheid, S. Thiele, *Energy Technol.* **2021**, *9*, 2100164; b) F. Waidhas, S. Haschke, P. Khanipour, L. Fromm, A. Görling, J. Bachmann, I. Katsounaros, K. J. J. Mayrhofer, O. Brummel, J. Libuda, *ACS Catal.* **2020**, *10*, 6831–6842; c) L. Fusek, V. Briega-Martos, M. Minichová, L. Fromm, E.

Franz, J. Yang, A. Görling, K. J. J. Mayrhofer, P. Wasserscheid, S. Cherevko, O. Brummel, J. Libuda, *J. Phys. Chem. Lett.* **2024**, *15*, 2529–2536.

[12] V. Schwaab, F. Hemauer, E. M. Freiberger, N. J. Waleska-Wellnhofer, H.-P. Steinrück, C. Papp, *J. Phys. Chem. C* **2023**, *127*, 11058–11066.

[13] a) Y. Sekine, T. Higo, *Top. Catal.* **2021**, *64*, 470–480; b) D. Zakgeym, Katalysator- und Prozessentwicklung für sauerstoffhaltige flüssige organische Wasserstoffträger-Systeme, PhD thesis, Friedrich-Alexander-Universität Erlangen-Nürnberg (DE), **2022**; c) N. Brückner, K. Obesser, A. Bösmann, D. Teichmann, W. Arlt, J. Dungs, P. Wasserscheid, *ChemSuSChem* **2014**, *7*, 229–235.

[14] M. Kinne, T. Fuhrmann, C. M. Whelan, J. F. Zhu, J. Pantförder, M. Probst, G. Held, R. Denecke, H. P. Steinrück, *J. Chem. Phys.* **2002**, *117*, 10852–10859.

[15] a) J. F. Zhu, M. Kinne, T. Fuhrmann, R. Denecke, H. P. Steinrück, *Surf. Sci.* **2003**, *529*, 384–396; b) J. Wulfes, A.-K. Baumann, M. Cieminski, C. Schröder, S. Schauermann, *J. Catal.* **2024**, *429*, 115213; c) F. Hemauer, U. Bauer, L. Fromm, C. Weiss, A. Leng, P. Bachmann, F. Düll, J. Steinhauer, V. Schwaab, R. Grzonka, A. Hirsch, A. Görling, H. P. Steinrück, C. Papp, *ChemPhysChem* **2022**, *23*, e202200199.

[16] S. Attia, S. Schauermann, *J. Phys. Chem. C* **2019**, *124*, 557–566.

[17] a) G. B. Fisher, J. L. Gland, *Surf. Sci.* **1980**, *94*, 446–455; b) H. Ogasawara, B. Brena, D. Nordlund, M. Nyberg, A. Pelmenschikov, L. G. Pettersson, A. Nilsson, *Phys. Rev. Lett.* **2002**, *89*, 276102.

[18] M. Kinne, T. Fuhrmann, J. F. Zhu, C. M. Whelan, R. Denecke, H. P. Steinrück, *J. Chem. Phys.* **2004**, *120*, 7113–7122.

[19] H. Cabibil, H. Ihm, J. M. White, *Surf. Sci.* **2000**, *447*, 91–104.

[20] C. T. Campbell, G. Ertl, H. Kuipers, J. Segner, *Surf. Sci.* **1981**, *107*, 207–219.

[21] P. A. Redhead, *Vacuum* **1962**, *12*, 203–211.

[22] a) K. Christmann, G. Ertl, T. Pignet, *Surf. Sci.* **1976**, *54*, 365–392; b) B. Poelsema, K. Lenz, G. Comsa, *J. Phys. Condens. Matter* **2010**, *22*, 304006.

[23] a) P. J. Feibelman, B. Hammer, J. K. Nørskov, F. Wagner, M. Scheffler, R. Stumpf, R. Watwe, J. Dumesic, *J. Phys. Chem. B* **2000**, *105*, 4018–4025; b) A. Patra, H. Peng, J. Sun, J. P. Perdew, *Phys. Rev. B* **2019**, *100*, 035332; c) K. G. Lakshmikanth, I. Kundappaden, R. Chatanathodi, *Surf. Sci.* **2019**, *681*, 143–148.

[24] T. Kachel, *J. large-scale Res. Facil. JLSRF* **2016**, *2*, A72.

[25] R. Denecke, M. Kinne, C. M. Whelan, H. P. Steinrück, *Surf. Rev. Lett.* **2002**, *9*, 797–801.

[26] C. Papp, H.-P. Steinrück, *Surf. Sci. Rep.* **2013**, *68*, 446–487.

[27] S. Doniach, M. Šunjić, *J. Phys. C: Solid State Phys.* **1970**, *3*, 285–291.

[28] F. Bondino, G. Comelli, F. Esch, A. Locatelli, A. Baraldi, S. Lizzit, G. Paolucci, R. Rosei, *Surf. Sci.* **2000**, *459*, L467–L474.

[29] P. Feulner, D. Menzel, *J. Vac. Sci. Technol.* **1980**, *17*, 662–663.

[30] F. Neese, *WIREs Comput. Mol. Sci.* **2022**, *12*, e1606. <

[31] J. P. Perdew, K. Burke, M. Ernzerhof, *Phys. Rev. Lett.* **1996**, *77*, 3865–3868.

[32] E. Caldeweyher, C. Bannwarth, S. Grimme, *J. Chem. Phys.* **2017**, *147*, 034112.

[33] a) G. Kresse, J. Furthmüller, *Phys. Rev. B* **1996**, *54*, 11169–11186; b) G. Kresse, J. Furthmüller, *Comput. Mater. Sci.* **1996**, *6*, 15–50; c) G. Kresse, D. Joubert, *Phys. Rev. B* **1999**, *59*, 1758–1775.

[34] a) S. Grimme, J. Antony, S. Ehrlich, H. Krieg, *J. Chem. Phys.* **2010**, *132*, 154104; b) S. Grimme, S. Ehrlich, L. Goerigk, *J. Comput. Chem.* **2011**, *32*, 1456–1465.

[35] M. Methfessel, A. T. Paxton, *Phys. Rev. B* **1989**, *40*, 3616–3621.

[36] P. E. Blöchl, O. Jepsen, O. K. Andersen, *Phys. Rev. B* **1994**, *49*, 16223–16233.